IEEE Access
Multidisciplinary ⋮ Rapid Review ⋮ Open Access Journal

Received February 4, 2022, accepted February 16, 2022, date of publication February 21, 2022, date of current version March 1, 2022.

Digital Object Identifier 10.1109/ACCESS.2022.3153083

Two-Dimensional RSSI-Based Indoor Localization Using Multiple Leaky Coaxial Cables With a Probabilistic Neural Network

JUNJIE ZHU[1], (Graduate Student Member, IEEE), PENGCHENG HOU[1], KENTA NAGAYAMA[1], YAFEI HOU[1], (Senior Member, IEEE), SATOSHI DENNO[1], (Member, IEEE), AND RIAN FERDIAN[2], (Member, IEEE)

[1]Graduate School of Natural Science and Technology, Okayama University, Okayama, 700-8530, Japan
[2]Faculty of Information Technology, Andalas University, Padang 25175, Indonesia

Corresponding author: Yafei Hou (yfhou@okayama-u.ac.jp)

This work was supported in part by JSPS KAKENHI under Grant 20K04484, and in part by the Telecommunications Advancement Foundation (TAF).

ABSTRACT Received signal strength indicator (RSSI) based indoor localization technology has its irreplaceable advantages for many location-aware applications. It is becoming obvious that in the development of fifth-generation (5G) and future communication technology, indoor localization technology will play a key role in location-based application scenarios including smart home systems, manufacturing automation, health care, and robotics. Compared with wireless coverage using conventional monopole antenna, leaky coaxial cables (LCX) can generate a uniform and stable wireless coverage over a long-narrow linear-cell or irregular environment such as railway station and underground shopping-mall, especially for some manufacturing factories with wireless zone areas from a large number of mental machines. This paper presents a localization method using multiple leaky coaxial cables (LCX) for an indoor multipath-rich environment. Different from conventional localization methods based on time of arrival (TOA) or time difference of arrival (TDOA), we consider improving the localization accuracy by machine learning RSSI from LCX. We will present a probabilistic neural network (PNN) approach by utilizing RSSI from LCX. The proposal is aimed at the two-dimensional (2-D) localization in a trajectory. In addition, we also compared the performance of the RSSI-based PNN (RSSI-PNN) method and conventional TDOA method over the same environment. The results show the RSSI-PNN method is promising and more than 90% of the localization errors in the RSSI-PNN method are within 1 m. Compared with the conventional TDOA method, the RSSI-PNN method has better localization performance especially in the middle area of the wireless coverage of LCXs in the indoor environment.

INDEX TERMS Leaky coaxial cable(LCX), localization, RSSI, neural network.

I. INTRODUCTION

In the last couple of years, due to the large-scale commercialization of the fifth-generation (5G) mobile communication technology and the explosive growth of the number of smart devices, various services and applications have emerged to change people's lives. Location-based services including outdoor positioning and navigation, proximity social networking, and image geotagging have become basic demands in recent years. The localization of users and devices is of great value in a wide range of fields such as autonomous vehicles [1], health care [2], industrial and manufacturing automation [3], and robotics [4]. It can also benefit many novel systems including Internet of Things (IoT) [5], Internet of Vehicles (IoV) [6], smart home system [7], smart building [8], etc.

Global positioning system (GPS) as the most widely used localization technology provides localization and navigation service for almost global users. However, the GPS is not effective or accurate in the indoor environment due to its poor reception of signals from satellites. Technologies of indoor localization, which do not need the GPS signal or direct access to the base station, are playing a key role in many indoor application scenarios. Systems for localization

The associate editor coordinating the review of this manuscript and approving it for publication was Shuihua Wang.

can realize the location detection of the target with the help of different tools. Methods based on proximity sensors (e.g., infrared sensors, motion sensors, and ultrasound sensors) can provide localization for target users, but usually, it is hard to share the location information directly to target users [9]. Localization methods based on wireless signals have been greatly advanced and can be well integrated into the wireless communication system [10]. In addition, using a magnetic induction-based approach can also improve the performance of localization [11]. In recent years, most researches on indoor localization consider the wireless communication system using conventional monopole antennas and it has two drawbacks. One is the requirement of many access points for wireless coverage in the linear-cell environment (a place that is long and narrow) such as a manufacturing factory, railway station, and underground shopping mall. Another is the large power attenuation of the signal power in the air. These two problems can be solved by using leaky coaxial cable (LCX) for wireless coverage. LCX which can be used as antennas has been researched for several years. The potential advantages promote LCX to play an important role in wireless communication for various applications especially in linear-cell environment. LCX can be installed simply and it has uniform coverage and low interference between cells [12]–[14]. Reference [15] shows the employment of LCX in wireless power transfer (WPT). LCX also can be employed to train and the train ground communication system [16]. In [17]–[20], authors find that it is possible to form a 2-by-2 multi-input multi-output (MIMO) channel using only one LCX due to its bi-directional radiation property. After that, reference [21] presents a 4-by-4 LCX-MIMO system using one composite LCX. In addition to the usage for wireless communication, LCX is available for localization in indoor environments [22]–[24]. References [22] and [23] propose the localization methods with time of arrival (TOA) and time difference of arrival (TDOA) in LCX systems. In [24], authors develop a different combination of multiple LCXs to achieve higher accuracy in localization. On the other hand, due to the constant power loss in the cable, LCX can easily improve the channel capacity by transmitting power allocation using the user's position information [25].

Recently, machine learning approaches have been widely explored and used in many fields. In localization technology, machine learning is often used to classify a large number of characteristic information of wireless signals from user devices to improve localization accuracy. The most commonly used signal characteristic information in localization includes received signal strength indicator (RSSI), angle of arrival (AOA), time of arrival (TOA), time difference of arrival (TDOA), and channel state information (CSI) [10]. From the perspective of low cost in hardware requirements and low computational complexity, the RSSI-based method is one of the simplest localization methods for indoor environments because of the easy measurement of RSSI value. Most recent studies have focused on the usage of neural networks (NN) and other classification algorithms to improve localization performance. Reference [26] shows an RSSI-based fingerprinting localization method using recurrent neural networks (RNNs) in an indoor environment. A convolutional neural network (CNN) based approach for indoor localization using RSS time-series from wireless local area network (WLAN) access points is presented in [27]. The authors also proposed a multi-layer neural network for RSSI-based localization in [28]. In addition, A novel k-nearest neighbor (KNN) algorithm based on RSSI similarity and position distances for indoor localization is proposed in [29].

The motivation of this paper is to propose an RSSI-based indoor localization approach by using LCX for indoor application environments such as smart logistics warehouses and automated factories. In the future, there will be large numbers of intelligent guided vehicles or robots that automatically move according to trajectories in these application scenarios. Different from unplanned movement, the RSSI of the signals transmitted by these mobile devices has a high correlation related to the location. Compared with the conventional method that uses the TDOA information to directly calculate the position, the method using NN can take advantage of the correlation of the time series data of the target's RSSI. For the RSSI-based localization method using LCX, a fundamental question is whether the time-series data obtained by LCX is more efficient to the correct estimation of target location than the localization accuracy of the conventional TDOA based methods. On the other hand, for two-dimensional (2-D) localization, at least two sets of TDOA data are required to calculate the target location, which means that we need two or more LCXs to complete this process [23]. However, for the method based on RSSI time-series data using NN, it can effectively reduce the number of LCXs as access points.

As a performance investigation for the RSSI-based indoor localization using LCX, we utilize a probabilistic neural network (PNN) to find locations using the RSSI data received by LCX in indoor environments. PNN is a feedforward network derived from the Bayesian network and is widely used in classification and pattern recognition problems [30]–[33]. The simplified architecture of the feedforward neural network offers lower difficulty in actual employment. Compared with other types of neural networks, the feedforward neural network has better performance when handling and processing nonlinear data under large data samples, and it does not require feature engineering in processing. The RSSI data samples are measured at the LCX side using a geometrically based single-bounce (GBSB) channel model with both of line-of-sight (LOS) propagation component and non-line-of-sight (NLOS) propagation component [34]. For comparison, we will also provide the localization performance of the TDOA-based method using LCX over the same environment. In summary, the main contributions of this paper are two-fold:

(1) A classical three-dimensional (3-D) channel model for LCX communication system in a multipath-rich indoor environment is established using a GBSB model

according to the radiation property of LCX. The RSSI data samples can be simulated by using the LCX channel model.

(2) We propose an RSSI-based indoor localization method using multiple LCXs with a PNN approach. Compared with the conventional TDOA method, the proposal improves the localization accuracy by machine learning RSSI data samples from LCXs. We provide numerical simulation experiments as a performance investigation for the proposal. The results show the performance of the RSSI-PNN method is promising and is better than the conventional TDOA method.

The rest of the paper is structured as follows. In Section II, we introduced the LCX radiation property and channel model. Then the conventional TDOA method and RSSI-based localization method using PNN are explained in Section III. Performance results of localization error are given in Section IV, and end the paper with simple conclusions in Section V.

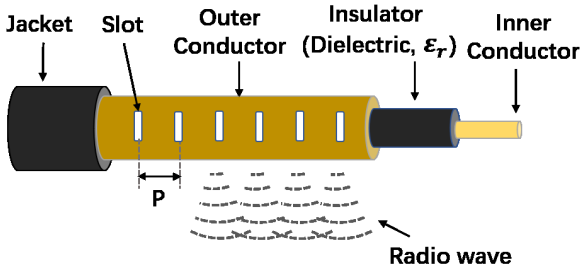

FIGURE 1. LCX structure.

II. LCX RADIATION PROPERTY AND CHANNEL MODEL

A. LCX STRUCTURE AND RADIATION PROPERTY

Fig. 1 shows the 4-layer structure of LCX used for wireless communication. Different from conventional coaxial cable, the slots arranged periodically over the outer conductor can be equivalent to a uniform linear array of magnetic dipole antennas and the radio waves can be radiated and received through these slots. The signal strength of LCX depends on its radio waves from all slots at the far-field region. Radiation angles with peak directivity of LCX can be expressed by

$$\theta_m = \sin^{-1}(\sqrt{\epsilon_r} + \frac{m\lambda}{P}), \quad (m = -1, -2, \ldots) \tag{1}$$

where m is the harmonic order, P is the period of slots and ϵ_r is the LCX's relative insulator permittivity. λ is the wavelength related to the frequency band. m is set as -1 to avoid radiated harmonics.

LCXs with different slot structures have different radiation properties. Fig. 2 shows two commonly used LCX types, one with vertical slots and the other with pair of inclined slots [25]. Fig. 2(a) is the radiation pattern of the H-type LCX and it can be regarded as an array of small monopole antennas. Due to the slot structure design, the V-type LCX in Fig. 2(b) has bi-directional radiation property if we input signals to both ends of the cable simultaneously [21]. In the conventional localization method, V-type LCX uses the signal radiation angle and TDOA value to estimate the location of the target user.

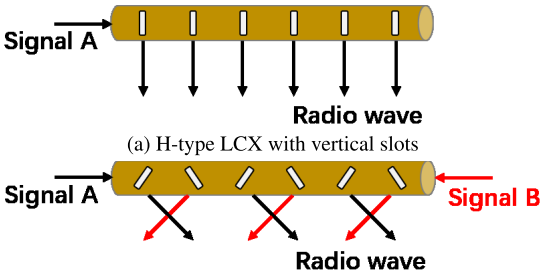

(a) H-type LCX with vertical slots

(b) V-type LCX with pair of inclined slots

FIGURE 2. Radiation patterns of different LCXs.

B. CHANNEL MODELING FOR LCX

In this paper, we provide a GBSB model using the basic theory in the communication field to establish a classical model for the LCX communication system. Let's take H-type LCX as an example and the V-type LCX can be modeled in the same way. The signal propagation from user to LCX can be divided into two parts the line-of-sight (LOS) component and the non-line-of-sight (NLOS) component.

We consider the received signal at the LCX side as S_{LCX} and it can be expressed as

$$S_{\text{LCX}} = S_{\text{LOS}} + S_{\text{NLOS}}, \tag{2}$$

where S_{LOS} is the LOS signal and S_{NLOS} is the NLOS signal. Here, S_{LOS} is deterministic process and S_{NLOS} is stochastic process. As Fig. 3(a) shows, the LOS propagation paths has two parts including the path from the user (Tx) to slot O_i in the air and the path from slot O_i to cable end in the cable. S_{LOS} depends on the superposition of LOS signals from all slots and can be simply expressed as

$$S_{\text{LOS}} = \sum_{i=1}^{N} S_{O_i}, \tag{3}$$

where N is the number of slots over LCX and S_{O_i} represents the signal from user Tx via slot O_i to the cable end. Due to the uniform power attenuation in the cable, the corresponding longitudinal amplitude attenuation of the signal in LCX can be represented as

$$\alpha_i = 10^{\frac{-\alpha P(i-1)}{20}}, \tag{4}$$

where α is the longitudinal amplitude attenuation constant per meter in LCX. P is the period of cable slots and $P(i-1)$ means the distance from slot O_i to the cable end. Similarly, the phase variations in LCX can be represented as

$$\beta_i = k_r P(i-1). \tag{5}$$

k_r is the propagation constant of electrical wave in LCX and $k_r = k_0\sqrt{\epsilon_r}$. k_0 is the propagation constant of electrical wave

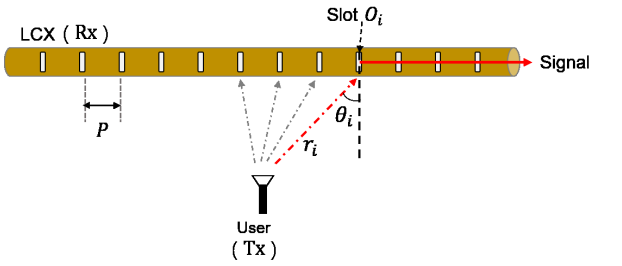

(a) Line-of-sight (LOS) component

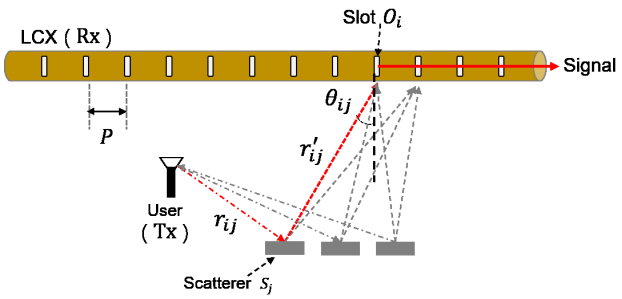

(b) Non-line-of-sight (NLOS) component

FIGURE 3. The LOS and NLOS propagation paths in the LCX channel model.

in free space and $k_0 = 2\pi f/c$. c is the speed of light. We can change the values of k_0 and k_r by assigning different values to f to simulate the generation of signals of different frequencies in free space and LCX. It assumes that user Tx is with one monopole antenna and the direct distance between the user and the center point of slot O_i is r_i. The LOS signal S_{LOS} can be expressed by

$$S_{\text{LOS}} = \sum_{i=1}^{N} \alpha_i \sqrt{P_l(r_i) \cdot E(\theta_i)} \cdot e^{-j(k_0 r_i + \beta_i)}. \quad (6)$$

$E(\theta_i)$ is the power gain due to the radiation angle [25]. Function $P_l(r_i)$ represents the pathloss at a distance of r_i in indoor environment over 2.4GHz band and can be expressed by

$$P_l(d) = 18.7 * \log_{10} d + 46.8 + 20 * \log_{10}(2.4/5), \quad (7)$$

where d is the distance of the propagation path.

Fig. 3(b) shows the NLOS component of the signal propagation. Similar to the LOS component, the NLOS signal S_{NLOS} can be simply expressed as

$$S_{\text{NLOS}} = \sum_{i=1}^{N} \sum_{j=1}^{M} S_{O_i S_j}. \quad (8)$$

Here, M is the number of the scatterers. $S_{O_i S_j}$ represents the signal from user Tx via scatterer S_j and slot O_i to cable end. We assume that the direct distance between Tx and scatterer S_j is r_{ij} and the distance between S_j and slot O_i is r'_{ij}. The NLOS signal can be calculated by

$$S_{\text{NLOS}} = \sum_{i=1}^{N} \sum_{j=1}^{M} \alpha_i \sqrt{P_l(r_{ij} + r'_{ij}) \cdot E(\theta_{ij})} \cdot e^{j\varphi_{ij}} \cdot e^{-j(k_0(r_{ij}+r'_{ij})+\beta_i)}, \quad (9)$$

where φ_{ij} is the i.i.d random variables with uniform distributions at $[0,2\pi)$.

In addition, the RSSI value of the LCX received signal can be calculated by:

$$RSSI_{\text{LCX}} = 20 * \log_{10}(|S_{\text{LCX}}(t)|). \quad (10)$$

III. LOCALIZATION METHODS USING LCX

A. RSSI DATA COLLECTION

We consider the indoor environment as a 3-D space similar to a factory as shown in Fig. 4. The user is considered as the transmitter moves on the trajectory. We collect the RSSIs at the LCX side and the user's location information as a data set for training and testing using PNN.

Fig. 4(a) is the overall view of the simulation model in a $24 \times 14 \times 3$ [m^3] space. We set 4 H-type LCXs (two LCXs are in 24 meters, two LCXs are in 14 meters) as the receivers Rx on the wall. The user Tx moves in a clockwise direction on the trajectory. It assumes that several scatterers are uniformly distributed in this space.

Fig. 4(b) shows the top view of the simulation model. The red line is the user's standard trajectory with a length of 20 m and a width of 10 m. The black line is the user's actual trajectory route with random deviation and the max deviation of the user from the standard trajectory is 0.5 m.

We use Fig. 4(c) to introduce the scatterer distribution pattern of the channel model. We divide the user's trajectory into 12 parts. The channel model considers different scatterer distribution patterns when the user is at different trajectory parts. For example, when the user is at part 1 of the trajectory, the channel model mainly considers the scattering points distributed near part 1. It should be noted that when the user turns in a corner, the distribution of scattering points in the same area will also changes. When the user is at the same part of the trajectory in each lap, the distribution of scattering points remains unchanged.

Fig. 4(d) shows the layout of the quantized locations and the measurement points for data samples. We partition the indoor space into blocks with a side length of 0.25 m. The side length represents the resolution of this localization scheme. We consider that the user moves on the trajectory at a speed of 1 m/s. The location of the user on the trajectory can be represented by (x, y) which is the coordinate of the center point of the block where the user is located. For the calculation of the RSSI value from each LCX at each measurement point, we take several frequency points by setting different frequency values with equal interval to f in the LCX channel model. These frequency points are centered at 2.4 GHz and it calculates the RSSI value at each frequency point using equations in Section II.B (Eq. (2), (6), (9), and (10)). Then, we obtain several RSSI values and take the average value as the final RSSI. We take 4 RSSIs from 4 LCXs at one measurement point as a data sample. The user's location (x, y) is also recorded at the same time. The sampling rate is set to 240 measurement points per lap on the trajectory. We finished the data sample collection after the user moved 300 laps and

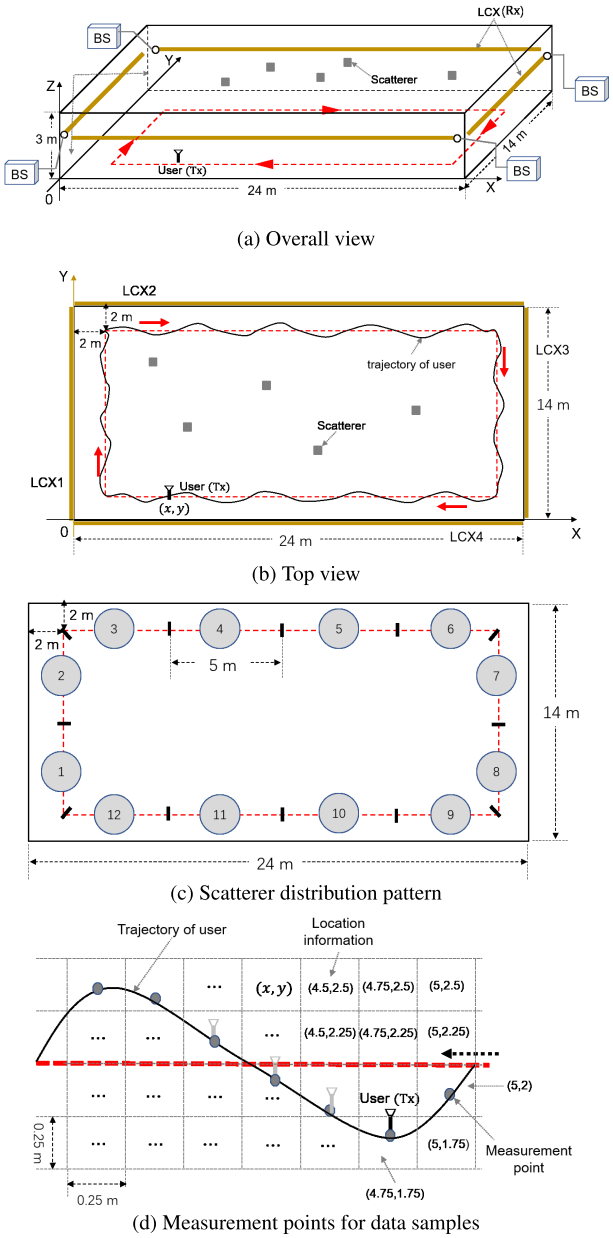

(a) Overall view

(b) Top view

(c) Scatterer distribution pattern

(d) Measurement points for data samples

FIGURE 4. Configuration of the channel model in indoor environment.

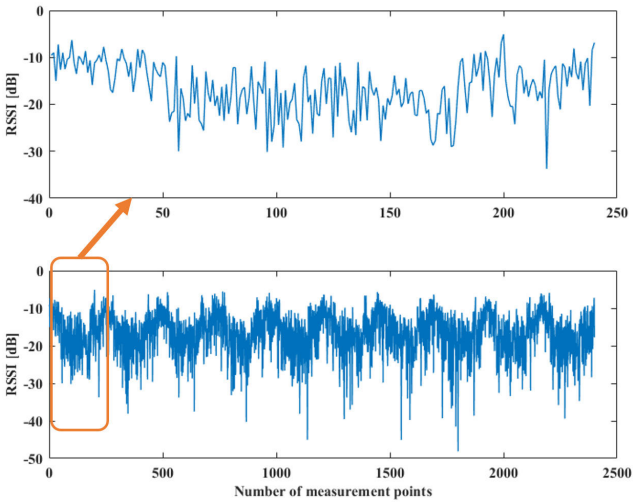

FIGURE 5. RSSI data samples.

TABLE 1. Simulation specifications for RSSI collection.

Parameter	Value
LCX type	H-type (for all)
LCX slot period P [m]	0.08 (for all)
Shortening coefficient in LCX	0.6403 (for all)
Cable loss [dB/m]	0.3 (for all)
Frequency bandwidth (frequency range) [MHz]	2 (2399-2401)
Interval between frequency points [KHz]	10
Number of receivers N_{L}	1, 2, 4
Number of scatterers M	10, 20, 50
LCX height [m]	1.5
User antenna height [m]	1
User output power [dBm]	20

a total of 72000 data samples were obtained. As a sample, we give the RSSI data values measured from one LCX in 1 and 10 laps respectively in Fig. 5.

In addition, we also tried to change the number of LCX antennas and scattering points to study the changes in localization performance. The specifications of the LCX and other detailed parameters and conditions in the simulation are listed in table 1.

B. PNN METHOD

PNN is a feedforward network that developed with the development of a radial basis function network. The PNN model is derived from the Bayesian network which is a statistical algorithm that uses the Kernel Fisher discriminant analysis techniques. The architecture of the PNN model as Fig. 6 shows is divided into four layers: input layer, pattern layer, summation layer, and output layer.

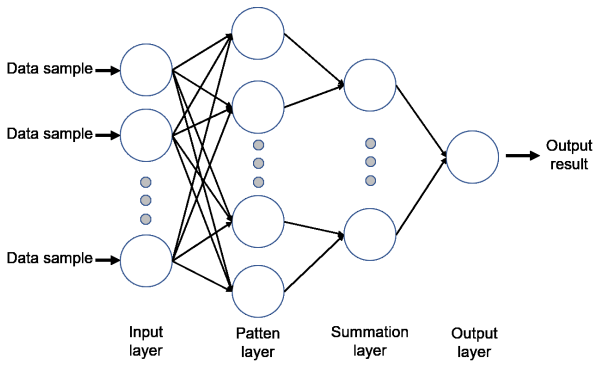

FIGURE 6. The architecture of PNN.

The input layer receives the training sample values and passes the vector to the pattern layer. The number of neurons in the input layer is equal to the dimension of the sample vector. In the pattern layer and summation layer, each neuron calculates the Euclidian distance between the incoming and reference vectors and multiplies the result with a Gaussian activation function. Then, the contribution of each classification c is summed by the neurons in the summation layer,

resulting in a probability as indicated:

$$P_c(x) = \frac{1}{\sigma_c\sqrt{2\pi}} \sum_{j=1}^{N_{E_C}} e^{-\frac{\|v-v_{c,j}\|^2}{2\sigma_c^2}}, \tag{11}$$

where v is the sample vector, vector $v_{c,j}$ is the jth training vector. The number of training vectors for class c is N_{E_C} and σ_c is the Gaussian spread. $||v - v_{c,j}||^2$ represents the squared Euclidean distance between the input and jth training vector of class c. In the output layer. it will select the class which has the highest probability.

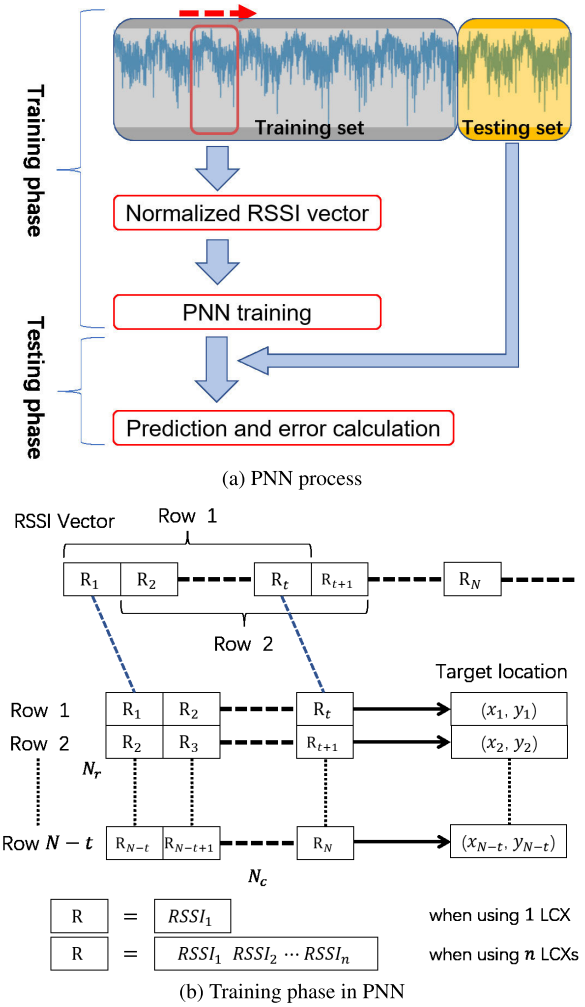

(a) PNN process

(b) Training phase in PNN

FIGURE 7. The process of RSSI-based PNN algorithm in localization.

We use Fig. 7 to give a brief introduction to the process of the PNN algorithm in this work. The whole process has two parts: the training phase and the testing phase. As it shows in Fig. 7(a), in the training phase, the RSSI data set is preprocessed into an RSSI vector and then input into the PNN network for training. In the testing phase, we input the RSSI of the test data set into the trained network, the PNN estimates the most likely classification of input data samples and the location prediction will be obtained. We calculate the localization error in the final step.

Fig. 7(b) shows the training phase in the PNN process. The vector receives RSSI samples recorded along the trajectory route is converted into stacked sliding windows each of length N_c samples. The stacked vectors then form a N_r (rows) $\times$ N_c (columns) predictor matrix as shown in Fig. 7. And the prediction target is the location of the user corresponding with the RSSI value. Each row of a corresponding length N_r target column vector contains the index that points to the end address of the fading sliding-window vector stored in memory. The PNN learns to associate each window with its start address during training. After training and during normal operation, the PNN returns the address index of the closest matching row that has the minimum Euclidean distance with the current observation vector.

The parameter settings of the PNN are listed in table 2.

TABLE 2. PNN settings.

Parameter	Value
Number of RSSI values in one sample	1, 2, 4
PNN column length N_c	240, 480, 960
PNN rows length N_r	54000
Sliding-window step size	1 sample
Number of neurons in pattern and summation layer	54000, 960
Number of training data samples	54000
Number of testing data samples	18000
Gaussian spread σ	0.1, 0.3, 0.5, 0.7, 1

C. TDOA METHOD

To compare with the proposed RSSI-based method Using PNN, we also provide an introduction to the conventional TDOA method. The main idea of the TDOA method in 2-D localization is to use the time difference between the signal reaching the two ends of the cable and the radiation angle of the signal to geometrically calculate the location information of the target user. Due to limited space, only the main content of the TDOA method using LCX is introduced here. The content in detail can be found in [23].

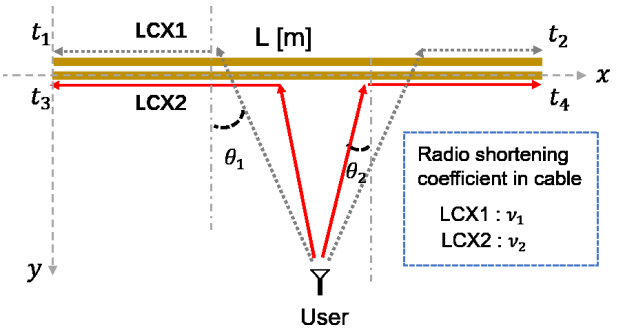

FIGURE 8. LCX localization using TDOA method.

Fig. 8 shows the scheme of the TDOA localization using two different parallel V-type LCXs (denoted as V1, V2) with different radiation angles. t_1, t_2, t_3, t_4 are the arrival time of signals, which is the time it takes for the signal to propagate from the user to the end of the LCX. Since the arrival time of signal t_1, t_2, t_3, t_4 can be calculated geometrically, the user location in the X-axis direction and the Y-axis direction can

be expressed as

$$x = \frac{\frac{1}{2}(t_1 - t_2)v_1 c + \frac{1}{2}(t_3 - t_4)v_2 c + L}{2} \tag{12}$$

$$y = \frac{\cos\theta_1 \cos\theta_2[v_1 v_2 c(t_1 - t_3) - x(v_2 - v_1)]}{v_1 v_2(\cos\theta_2 - \cos\theta_1) - v_2 \sin\theta_1 \cos\theta_2 + v_1 \sin\theta_2 \cos\theta_1}. \tag{13}$$

L is the length of the LCX. v_1 and v_2 are the shortening coefficients of the radio waves in LCX1 and LCX2. θ_1 and θ_2 are the maximum radiation angles of the LCXs. For the arrival time estimation of the signal, we use the multiple signal classification (MUSIC) algorithm which is a relatively simple and efficient eigenstructure method [23]. MUSIC algorithm estimates the noise subspace from available samples and searches for steering vectors that are as orthogonal to the noise subspace as possible. This is normally accomplished by searching for peaks in the signal spectrum.

Here, we give a brief introduction to the TDOA measurement using the MUSIC algorithm. Given an $K \times K$ autocorrelation matrix from the signal samples at different frequency f as

$$\begin{aligned} \mathbf{Rx} &= \sum_{i=1}^{K} u_i \mathbf{V}_i \mathbf{V}_i^H \\ &= \sum_{i=1}^{s} (\lambda_i + \sigma_w^2)\mathbf{V}_i \mathbf{V}_i^H + \sum_{i=s+1}^{K} \sigma_w^2 \mathbf{V}_i \mathbf{V}_i^H, \end{aligned} \tag{14}$$

where the u_i and $\mathbf{V}_i$ are the eigenvalue and the eigenvector corresponding to the eigenvalue. The superscript H represents the Hermitian transpose. λ_i is the eigenvalue corresponding to signal and σ_w^2 is the variance of white noise. The eigenvectors corresponding to the s largest eigenvalues span the signal subspace. The remaining $K - s$ eigenvectors span the orthogonal noise space. We define the estimation function for MUSIC as

$$g(\tau) = \frac{1}{\sum_{i=s+1}^{K} \left|\mathbf{V}_i^H \mathbf{e}(\tau)\right|^2}, \tag{15}$$

where $\mathbf{e}(\tau)$ is known as the steering vector and can be expressed as

$$\mathbf{e}(\tau) = \left[1, e^{-j2\pi f_1 \tau}, e^{-j2\pi f_2 \tau}, \cdots, e^{-j2\pi f_K \tau}\right]^T, \tag{16}$$

$$\tau = nT_r, \quad (n = 0, 1, 2, \cdots, N_s - 1). \tag{17}$$

T_r is the time resolution of the MUSIC method. N_s is the number of elements in the pseudo spectrum. The orthogonality between the noise subspace and the steering vectors will minimize the denominator in Eq. (15) to 0 value. However, it is a small value in practice due to the noise. As a result, it will give rise to a peak, which corresponds to the signal arrival, in $g(\tau)$. From that, we can estimate the TOA of signals and then calculate the TDOA value.

The TDOA-based localization method using LCX is usually used in a linear-cell environment. In the previous research, the authors used two LCXs to perform the localization with TDOAs and the experimental results show that the localization performance is not promising when the target user is far away from the LCXs [23]. So, for the performance investigation in the large space in this work, we use two parallel V-type LCXs (V1, V2) as a group on each wall in the simulation model in Fig. 4. A total of eight LCXs are placed on four walls to cover the user's trajectory area to ensure the localization performance of the TDOA method. The LCXs on each side only locate the user on an adjacent trajectory. The specifications of the LCX and other detailed parameters and conditions in the simulation are listed in table 3.

TABLE 3. Simulation specifications for TDOA method.

Parameter	Value
LCX type	V-type (V1, V2)
LCX slot period P [m]	0.04 (V1), 0.03 (V2)
Maximum radiation angle [deg]	18 (V1), 55 (V2)
Shortening coefficient in LCX	0.6403 (for all)
Cable loss [dB/m]	0.6 (for all)
Frequency bandwidth (frequency range) [MHz]	76.25 (2403.9-2480.15)
Interval between frequency points [KHz]	312.5
Number of receivers N_{L}	8 (4 for V1, 4 for V2)
Number of scatterers M	10
LCX height [m]	1.5
User antenna height [m]	1
User output power [dBm]	20

IV. LOCALIZATION PERFORMANCE

A. LOCALIZATION ERROR

1) LOCALIZATION ERROR IN RSSI-BASED PNN METHOD

The RSSI-based PNN (RSSI-PNN) method in this paper formulates localization as a classification problem. As stated in the previous section, we partition the indoor space into multiple blocks. The difference between the block predicted by the PNN algorithm and the actual block where the user is located will be quantified into a specific distance as the localization error. We use Fig. 9 to introduce the localization error quantification. If the predicted block happens to be the block where the user is located, the localization error is below d_1. If the predicted block is next to the user's block, the localization error is below d_2. Similarly, the maximal localization errors are quantified as $d_3, d_4, d_5, \ldots d_n$ when the predicted block is not the same as the user's one. It should be noted here that in the final experimental results we only provide the maximal value of the localization error as the performance of the RSSI-PNN method.

2) LOCALIZATION ERROR IN TDOA METHOD

In the TDOA method, the user's location is directly calculated by using the signal's TDOA and radiation angle, so we calculate the direct distance between the estimated location and the actual user location as the localization error.

B. RESULTS OF LOCALIZATION ERROR

The results of the localization error are shown by cumulative distribution function (CDF).

Fig. 10 shows the results of the localization error of the RSSI-PNN method using different numbers of LCXs. N_{L} is the number of LCXs. We also provided the results using the

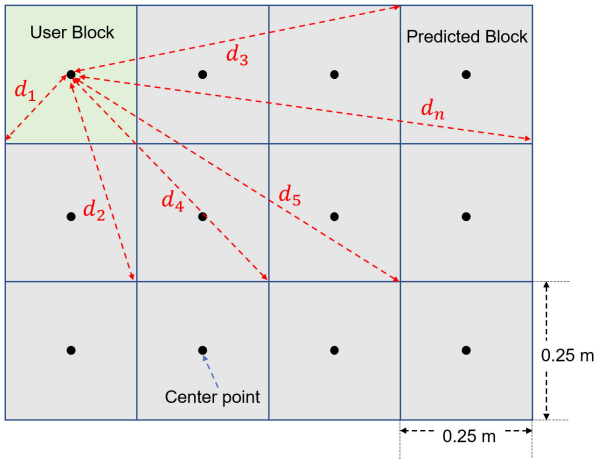

FIGURE 9. The maximal localization error for quantized locations in RSSI-based PNN method.

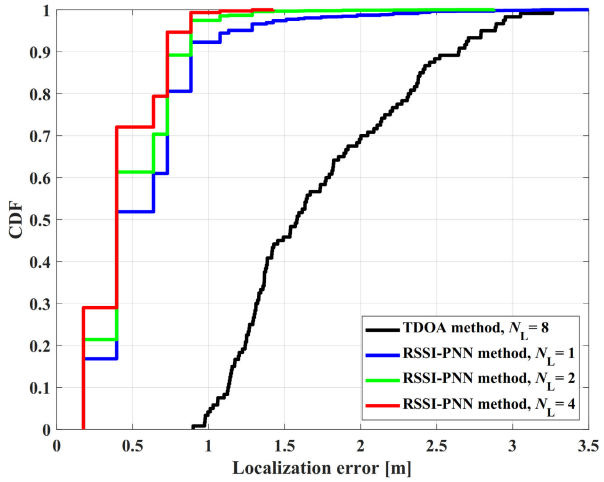

FIGURE 10. The comparison of the localization errors. (Number of scatterers $M = 10$).

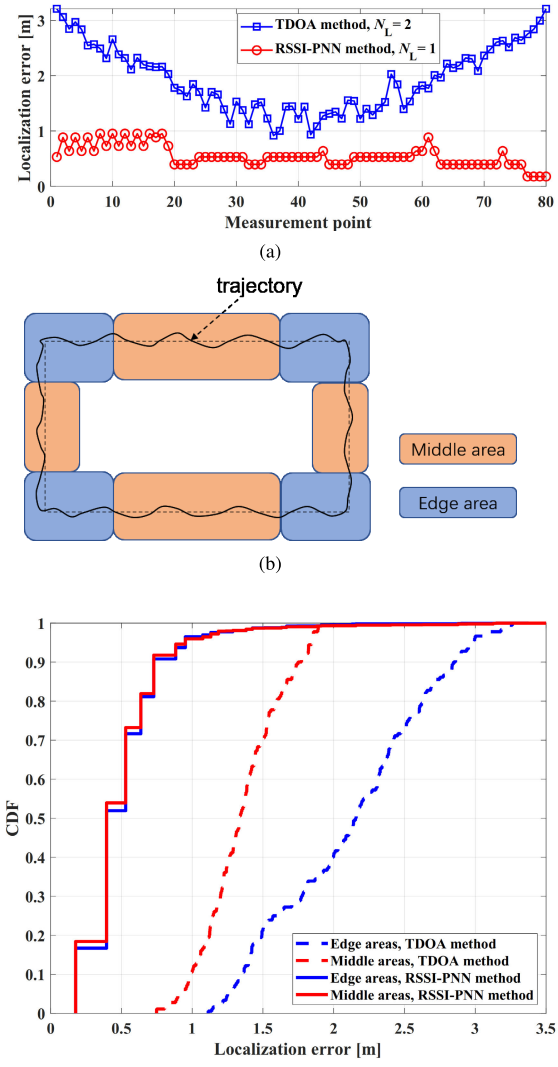

FIGURE 11. Localization errors in different areas. (a) Localization errors on the long side of the trajectory in one lap. (b) Area division of trajectory (c) Distribution of localization errors in different areas of trajectory. (Number of scatterers $M = 10$).

TDOA method for comparison. The number of scatterers M is set as 10. We can find that the localization performance of the RSSI-PNN method is better than that of the TDOA method. The blue and green lines in Fig. 10 represent the localization error of RSSI-PNN when using only one LCX (LCX2 in Fig. 4(b)) and when using two LCXs (LCX1 and LCX2 in Fig. 4(b)). We can see that the localization accuracy is improved when we increase the number of LCXs as the receivers in the RSSI-PNN method. In addition, more than 90% of the localization errors in the RSSI-PNN method are within 1m.

For the analysis of the difference in localization performance between the RSSI-PNN method and the TDOA method, we extract the localization errors of some areas of the user's trajectory. Fig. 11(a) shows the localization errors of two methods on the long side of the trajectory in one lap. The localization errors of the TDOA method are promising in the middle part of the trajectory. However, the gap in the localization performance between the two methods becomes large in the edge part. In addition, we divide the trajectory into middle area and edge area as Fig. 11(b) shows. Both middle area and edge area contain 120 measurement points at the trajectory per lap. Fig. 11(c) shows the distribution of localization errors in different areas of trajectory. In the TDOA method, 70% of the localization error in the middle area is below 1.5 m and 80% of the localization error in the edge area is over 1.5 m. The main reasons for the different performance of the TDOA method are the signal's radiation angle error and the low resolution of the MUSIC algorithm for detecting the arrival signal. On the contrary, the RSSI-PNN method can avoid these problems.

Multipath of signal in the indoor environment is also one of the important factors affecting wireless communication and localization. In this paper, we also investigate the localization performance under different numbers of scatterers. As it shows in Fig. 12, when using the same number of LCXs, the localization performance becomes worse when

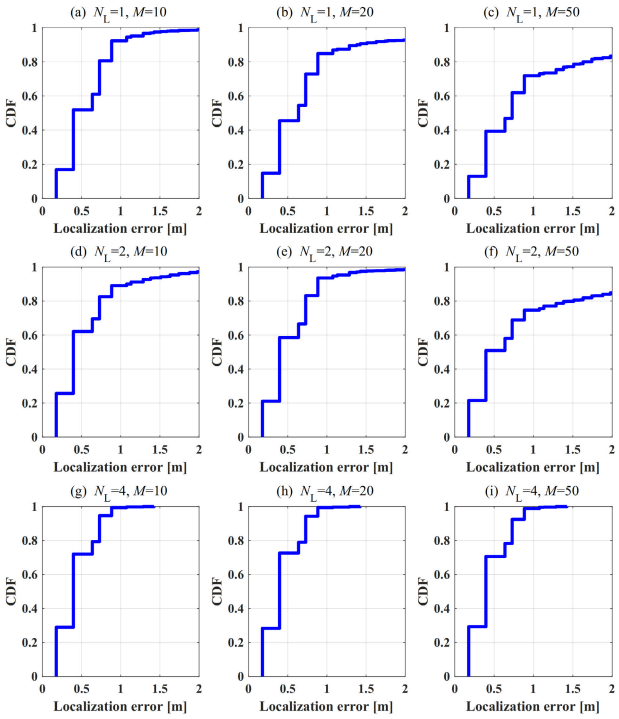

FIGURE 12. The CDF of Localization error under different number of scatterers.

the scatterers increase. However, the influence of multipath gradually becomes smaller as the number of LCXs increases.

Fig. 13 is the localization performance of the RSSI-based methods using different Gaussian spread σ values in PNN training. In PNN, if the spread value is near zero, the network acts as a nearest neighbor classifier. As the spread value becomes larger, the designed network takes into account several nearby design vectors. When utilizing RSSI data from one or two LCXs, the prediction performance is promising as the spread value approaches 0. However, when utilizing RSSI data from four LCXs, the prediction performance becomes worse at a low spread value as shown in the localization performance when $\sigma = 0.1$ in Fig. 13(c). This may be caused by overfitting in PNN training. It is important to adjust the value of σ appropriately to keep the prediction performance when utilizing RSSI data from multiple LCXs. For overfitting or overtraining, we may avoid the problem by adopting a considerable amount of RSSI samples in the training phase and using another fraction of datasets for the testing phase [35]. This will be our future work in future research.

The resolution of the localization method in this work can be changed by adjusting the side length of the blocks in Fig. 4(d). As an investigation of the effect of localization resolution on performance, we provide localization results with a resolution of 0.5 m and 0.125 m in the simulation experiment for comparison. Fig. 14(a) shows the mean error (ME) of localization with different resolution patterns (pattern A, B, C is 0.5 m, 0.25 m, 0.125 m respectively). The average localization errors of resolution patterns A, B, and C are 1.36 m, 0.69 m, 0.43 m respectively. When the localization resolution

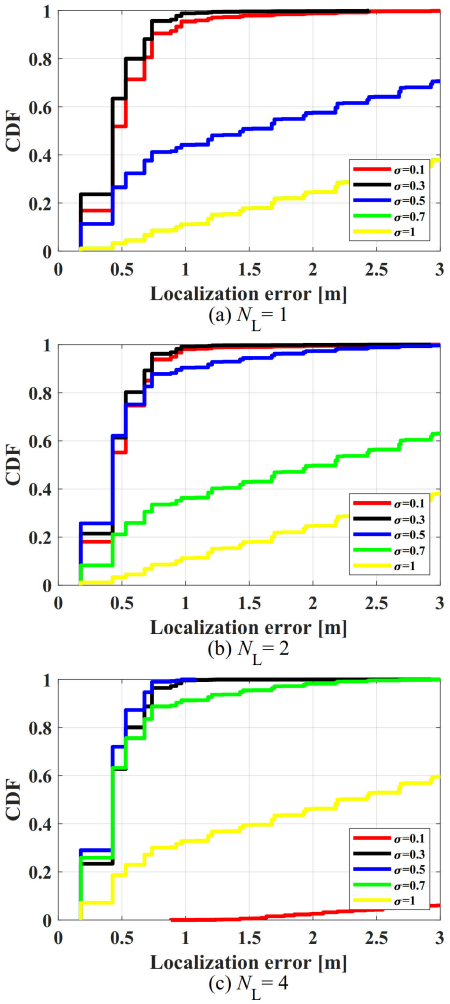

FIGURE 13. Localization error with different Gaussian spread values.

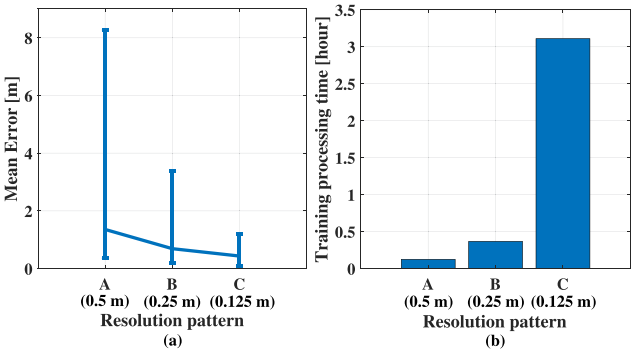

FIGURE 14. Localization error and training processing time at different resolution pattern. (Number of scatterers $M = 10$, Number of LCX $N_L = 1$).

changes, not only does the minimum distance between the measurement points become smaller, but the number of measurement points within the unit distance increases. So that the N_c (the size of the input layer in the PNN structure) in the PNN training model in Fig. 7(b) changes in size. For example, when the resolution is changed from 0.5m to 0.25m, the number of measurement points per unit distance is doubled, and N_c is doubled. As a result, the amount of

TABLE 4. Summary of simulation results with different resolution patterns.

Resulation pattern	ME	MSE	Training processing time (h)
A (0.5 m)	1.36	3.862	0.125
B (0.25 m)	0.69	0.6186	0.367
C (0.125 m)	0.43	0.2049	3.109

RSSI data is doubled, so the prediction performance of the PNN model can be improved. Since the training data size will be different due to different resolutions, we also provide the processing time of the data training at each resolution in Fig. 14(b). The summary of the simulation results including mean-square error (MSE) can be found in Table. 4. From the results, we can find that increasing the resolution can slightly improve the localization accuracy and performance, but it will greatly increase the training processing time.

V. CONCLUSION

The motivation of this paper is to propose an RSSI-based indoor localization approach by using the PNN algorithm in the LCX system. The proposal is aimed at the two-dimensional localization of the user in a trajectory. We present a GBSB model for the LCX system and simulate the RSSIs received by multiple LCXs. By training and testing the RSSI time-series data, we investigate the localization performance of the RSSI-PNN method in the LCX system. We also provide the localization performance of the TDOA method for comparison. The results show the RSSI-PNN method is promising and performs better than the TDOA method. Furthermore, the RSSI-PNN method can reduce the number of LCXs used for localization.

It will be our future work to improve the algorithm and localization accuracy of the localization method in the LCX system. In addition, we will also study the performance of the RSSI-PNN approach using LCX in a real environment.

REFERENCES

[1] S. Kuutti, S. Fallah, K. Katsaros, M. Dianati, F. Mccullough, and A. Mouzakitis, "A survey of the state-of-the-art localization techniques and their potentials for autonomous vehicle applications," *IEEE Internet Things J.*, vol. 5, no. 2, pp. 829–846, Apr. 2018.

[2] J. Wyffels, J. D. Brabanter, P. Crombez, P. Verhoeve, B. Nauwelaers, and L. D. Strycker, "Distributed, signal strength-based indoor localization algorithm for use in healthcare environments," *IEEE J. Biomed. Health Informat.*, vol. 18, no. 6, pp. 1887–1893, Nov. 2014.

[3] G. Li, Y. Huang, X. Zhang, C. Liu, W. Shao, L. Jiang, and J. Meng, "Hybrid maps enhanced localization system for mobile manipulator in harsh manufacturing workshop," *IEEE Access*, vol. 8, pp. 10782–10795, 2020.

[4] H. Liu, F. Sun, B. Fang, and X. Zhang, "Robotic room-level localization using multiple sets of sonar measurements," *IEEE Trans. Instrum. Meas.*, vol. 66, no. 1, pp. 2–13, Jan. 2017.

[5] L. Militano, G. Araniti, M. Condoluci, I. Farris, and A. Iera, "Device-to-device communications for 5G Internet of Things," *EAI Endorsed Trans. Internet Things*, vol. 15, no. 1, pp. 1–15, 2015.

[6] O. Kaiwartya, A. H. Abdullah, Y. Cao, A. Altameem, M. Prasad, C.-T. Lin, and X. Liu, "Internet of vehicles: Motivation, layered architecture, network model, challenges, and future aspects," *IEEE Access*, vol. 4, pp. 5356–5373, 2016.

[7] V. Bianchi, P. Ciampolini, and I. De Munari, "RSSI-based indoor localization and identification for ZigBee wireless sensor networks in smart homes," *IEEE Trans. Instrum. Meas.*, vol. 68, no. 2, pp. 566–575, Feb. 2019.

[8] F. Zafari, I. Papapanagiotou, and K. Christidis, "Microlocation for Internet-of-Things-equipped smart buildings," *IEEE Internet Things J.*, vol. 3, no. 1, pp. 96–112, Feb. 2016.

[9] F. Gu, X. Hu, M. Ramezani, D. Acharya, K. Khoshelham, S. Valaee, and J. Shang, "Indoor localization improved by spatial context—A survey," *ACM Comput. Surveys*, vol. 52, no. 3, pp. 1–35, May 2020.

[10] F. Zafari, A. Gkelias, and K. K. Leung, "A survey of indoor localization systems and technologies," *IEEE Commun. Surveys Tuts.*, vol. 21, no. 3, pp. 2568–2599, 3rd Quart., 2017.

[11] S.-C. Lin, A. A. Alshehri, P. Wang, and I. F. Akyildiz, "Magnetic induction-based localization in randomly deployed wireless underground sensor networks," *IEEE Internet Things J.*, vol. 4, no. 5, pp. 1454–1465, Oct. 2017.

[12] Y.-T. Pan, G.-X. Zheng, and C. Oestges, "Characterization of polarized radio channel with leaky coaxial cable in a tunnel-like environment," *IEEE Antennas Wireless Propag. Lett.*, vol. 16, pp. 2803–2807, 2017.

[13] Y. Wu, G. Zheng, and T. Wang, "Performance analysis of MIMO transmission scheme using single leaky coaxial cable," *IEEE Antennas Wireless Propag. Lett.*, vol. 16, pp. 298–301, 2016.

[14] Z. Siddiqui, M. Sonkki, M. Tuhkala, and S. Myllymaki, "Periodically slotted coupled mode leaky coaxial cable with enhanced radiation performance," *IEEE Trans. Antennas Propag.*, vol. 68, no. 11, pp. 7595–7600, Nov. 2020.

[15] T. Okamoto, Q. T. Duong, T. Higashino, and M. Okada, "A proposal of data transmission in parallel line fed wireless power transfer," in *Proc. 15th Int. Symp. Commun. Inf. Technol. (ISCIT)*, Oct. 2015, pp. 85–88.

[16] D. G. Dudley, M. Lienard, S. F. Mahmoud, and P. Degauque, "Wireless propagation in tunnels," *IEEE Antennas Propag. Mag.*, vol. 49, no. 2, pp. 11–26, Apr. 2007.

[17] Y. Hou, S. Tsukamoto, M. Ariyoshi, K. Kobayashi, T. Kumagai, and M. Okada, "Performance comparison for 2 by 2 MIMO system using single leaky coaxial cable over WLAN frequency band," in *Proc. Signal Inf. Process. Assoc. Annu. Summit Conf. (APSIPA), Asia–Pacific*, Dec. 2014, pp. 1–6.

[18] S. Tsukamoto, T. Maeda, M. Ariyoshi, Y. Hou, K. Kobayashi, and T. Kumagai, "An experimental evaluation of 2 × 2 MIMO system using closely-spaced leaky coaxial cables," in *Proc. Signal Inf. Process. Assoc. Annu. Summit Conf. (APSIPA), Asia–Pacific*, Dec. 2014, pp. 1–6.

[19] Y. Hou, S. Tsukamoto, T. Maeda, M. Ariyoshi, K. Kobayashi, T. Kumagai, and M. Okada, "Configuration of MIMO system using single leaky coaxial cable for linear cell environments," *IEICE Commun. Exp.*, vol. 4, no. 5, pp. 143–148, May 2015.

[20] Y. Hou, S. Tsukamoto, S. Li, T. Higashino, K. Kobayashi, and M. Okada, "Capacity evaluation of MIMO channel with one leaky coaxial cable used as two antennas over linear-cell environments," *IEEE Trans. Veh. Technol.*, vol. 66, no. 6, pp. 4636–4646, Jun. 2017.

[21] Y. Hou, S. Tsukamoto, M. Ariyoshi, K. Kobayashi, and M. Okada, "4-by-4 MIMO channel using two leaky coaxial cables (LCXs) for wireless applications over linear-cell," in *Proc. IEEE 3rd GCCE*, Oct. 2014, pp. 125–126.

[22] T. Higashino, M. Okada, T. Maeda, and S. Tsukamoto, "An evaluation of error performance of position location in the LCX liner cell MIMO system," in *Proc. Int. Tech. Conf. Circuits/Syst. Comput. Commun.*, pp. 749–751, Jul. 2014.

[23] S. Oki, Y. Hou, T. Higashino, and M. Okada, "Two-dimensional positioning for radio terminal in 4-by-4 MIMO system using leaky coaxial cable antenna," *ITE Technique Rep.*, vol. 39, no. 4, pp. 45–48, Jan. 2015.

[24] J. Zhu, P. Hou, Y. Hou, S. Denno, and M. Okada, "A study for 2-D indoor localization using multiple leaky coaxial cables," *APSIPA Trans. Signal Inf. Process.*, vol. 9, no. 1, pp. 1–8, 2020.

[25] Y. Hou, J. Zhu, S. Denno, and M. Okada, "Capacity of 4-by-4 MIMO channel using one composite leaky coaxial cable with user position information," *IEEE Trans. Veh. Technol.*, vol. 68, no. 11, pp. 11042–11051, Nov. 2019.

[26] M. T. Hoang, B. Yuen, X. Dong, T. Lu, R. Westendorp, and K. Reddy, "Recurrent neural networks for accurate RSSI indoor localization," *IEEE Internet Things J.*, vol. 6, no. 6, pp. 10639–10651, Sep. 2019.

[27] M. Ibrahim, M. Torki, and M. ElNainay, "CNN based indoor localization using RSS time-series," in *Proc. IEEE Symp. Comput. Commun. (ISCC)*, Jun. 2018, pp. 1044–1049.

[28] H. Dai, W. Ying, and J. Xu, "Multi-layer neural network for received signal strength-based indoor localisation," *IET Commun.*, vol. 10, no. 6, pp. 717–723, Apr. 2016.

[29] B. Wang, X. Gan, X. Liu, B. Yu, R. Jia, L. Huang, and H. Jia, "A novel weighted KNN algorithm based on RSS similarity and position distance for Wi-Fi fingerprint positioning," *IEEE Access*, vol. 8, pp. 30591–30602, 2020.
[30] Y. Sun, J. Chen, C. Yuen, and S. Rahardja, "Indoor sound source localization with probabilistic neural network," *IEEE Trans. Ind. Electron.*, vol. 65, no. 8, pp. 6403–6413, Aug. 2018.
[31] A. K. Abed and D. I. Abdel-Qader, "A spatial voting approach for indoor positioning system using PNN-multiclassifier based on multiple SSIDs," in *Proc. IEEE 9th Annu. Comput. Commun. Workshop Conf. (CCWC)*, Jan. 2019, pp. 233–239.
[32] J. Webber, N. Suga, S. Ano, Y. Hou, A. Mehbodniya, T. Higashimori, K. Yano, and Y. Suzuki, "Machine learning-based RSSI prediction in factory environments," in *Proc. 25th Asia–Pacific Conf. Commun. (APCC)*, Nov. 2019, pp. 195–200.
[33] K. Zhang, F. Zhang, G. Zheng, and A. Saleem, "GBSB model for MIMO channel using leaky coaxial cables in tunnel," *IEEE Access*, vol. 7, pp. 67646–67655, 2019.
[34] L. B. label ref Miguel and F. Casadevall, "Time-domain model of spectrum usage for the analysis, design, and simulation of cognitive radio networks," *IEEE Trans. Veh. Technol.*, vol. 62, no. 5, pp. 2091–2104, Jun. 2013.
[35] S. Q. Mahdi, S. K. Gharghan, and M. A. Hasan, "FPGA-based neural network for accurate distance estimation of elderly falls using WSN in an indoor environment," *Measurement*, vol. 167, Jan. 2021, Art. no. 108276.

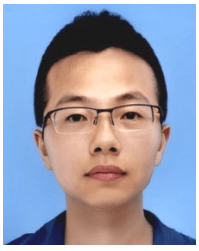

JUNJIE ZHU (Graduate Student Member, IEEE) was born in Jiangsu, China. He received the B.E. degree in communication engineering from the Nanjing University of Information Science and Technology, Nanjing, China, in 2016, and the M.E. degree from the Department of Natural Science and Technology, Okayama University, Japan, where he is currently pursuing the Ph.D. degree. His research interests include wireless communication and signal processing.

PENGCHENG HOU was born in Beijing, China. He received the B.E. degree in communication engineering from Hunan University, Changsha, China, in 2019. He is currently pursuing the M.E. degree with the Department of Natural Science and Technology, Okayama University, Japan. His research interests include wireless communication and signal processing.

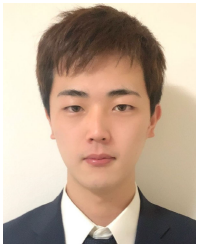

KENTA NAGAYAMA was born in Kagawa, Japan. He is currently studying at Okayama University. His research interests include wireless communication and signal processing.

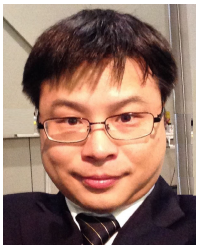

YAFEI HOU (Senior Member, IEEE) received the Ph.D. degrees from Fudan University, China, and the Kochi University of Technology (KUT), Japan, in 2007. He was a Postdoctoral Research Fellow at Ryukoku University, Japan, from August 2007 to September 2010. He was a Research Scientist at Wave Engineering Laboratories, ATR Institute International, Japan, from October 2010 to March 2014, where he has been a Guest Research Scientist, since October 2016. He was an Assistant Professor at the Graduate School of Information Science, Nara Institute of Science and Technology, Japan, from April 2014 to March 2017. He has been an Assistant Professor with the Graduate School of Natural Science and Technology, Okayama University, Japan, since April 2017. His research interests include communication systems, wireless networks, and signal processing. He received the Institute of Electronics, Information and Communication Engineers (IEICE) Communications Society Best Paper Awards, in 2016 and 2020, and the Best Tutorial Paper Award, in 2017. He serves as the member of the Editorial Board for IEEE Consumer Technology Society News on Consumer Technology (NCT) and the Associate Editor of IEEE Access. He is a member of IEICE.

SATOSHI DENNO (Member, IEEE) received the M.E. and Ph.D. degrees from Kyoto University, Kyoto, Japan, in 1988 and 2000, respectively. He was at the NTT Radio Communications Systems Laboratories, Yokosuka, Japan, in 1988 and 1997. From 2000 to 2002, he worked for NTT DoCoMo, Yokosuka. In 2002, he was at the DoCoMo Communications Laboratories Europe GmbH, Germany. From 2004 to 2011, he was an Associate Professor at Kyoto University. Since 2011, he has been a Full Professor with the Graduate School of Natural Science and Technology, Okayama University. His research interests include digital mobile radio communications, channel equalization, array signal processing, space-time codes, spatial multiplexing, and multimode reception. He received the Excellent Paper Award from the IEICE, in 1995, and the IEICE Communications Society Best Paper Awards, in 2020.

RIAN FERDIAN (Member, IEEE) received the B.S. and M.S. degrees *(cum laude)* in electrical engineering from the School of Electrical Engineering and Informatics, Institut Teknologi Bandung, Indonesia, in 2008 and 2012, respectively, and the Ph.D. degree from the Graduate School of Information Science, Nara Institute of Science and Technology, Nara, Japan, in 2017. He is currently a Lecturer with the Faculty of Information Technology, Universitas Andalas, Indonesia, since April 2014. His research interests include circuits for telecommunication systems, digital broadcasting technologies, and digital signal processing.